Accepted 11.11.15

Length and α-Fe Content Control of Self-Organised Ferromagnetic Nanowires Encapsulated by Multiwalled Carbon Nanotubes by Low Flow-Rate CVD.

Taze Peci and Mark Baxendale*

School of Physics and Astronomy, Queen Mary University of London, Mile End Road, London E1 4NS, UK

Abstract

Self-organised ferromagnetic nanowires encapsulated by multiwalled carbon nanotubes produced by CVD methods based on the thermal decomposition of ferrocene commonly contain the elemental phases: α-Fe, γ-Fe, and the carbide Fe_3C. A continuous α-Fe nanowire and control of nanowire and nanotube length and diameter are desirable. High α-Fe nanowire content has been achieved through synthesis temperature modification, vapour flow-rate, and post-synthesis heat treatment. Length and diameter are intimately related to the self-organisational growth processes; reported approaches include regulation of the vapour supply to minimise dispersion in the nucleation process and introduction of other growth-modifying precursor elements. High vapour flow-rate produces downstream fluctuation resulting in discontinuous nanowires and diameter dispersion, or external decoration with spherical particles, results from rapid evaporation of the ferrocene precursor. We report a low vapour flow-rate and constant evaporation temperature method which achieves continuous α-Fe nanowires on the same scale as the nanotube for lengths >10 μm without the necessity of post-synthesis heat-treatment or introduction of other precursor elements. The low vapour

*Corresponding author. Email address: m.baxendale@qmul.ac.uk (Mark Baxendale)

flow-rate regime has the advantage of sustaining the intrinsic temperature gradient at the tip of the forming structure which drives the vapour feedstock to the growth front to guarantee continuous nanowire formation.

1. Introduction

Ferromagnetic nanowires encapsulated by multiwalled carbon nanotubes are synthesised by CVD methods in which the species produced by the thermal decomposition of metallocenes provide nucleating metal droplets and the chemical feedstock for self-organised growth of structures perpendicular to an inert substrate at elevated temperature [1-18]. Such *in situ* carbon nanotube filling restricts the ferromagnetic nanowire to those transition metals (and alloys thereof) which catalyse the hydrocarbon decomposition and graphitic carbon formation that are central to the self-organisational process (Fe, Ni, Co). Confinement of the nanowire within the central capillary of the nanotube can result in unusual compositions not readily obtainable in the bulk. The carbon nanotube chemically passivates the nanowire and prevents its mechanical degradation. Applications follow from the ability to tune the magnetic response through the composition and shape anisotropy of the nanowire [19]: microwave absorption materials [20], nanocomposite filler particles [21], biomedical [22-27], nanoscale inductors [28], magnetic force microscopy probes [29], and magnetic paper [30].

The majority of effort has focussed on encapsulation of elemental α- Fe, owing to both the characteristically high saturation magnetisation and coercivity, by thermal decomposition of ferrocene (Fe $(C_5H_5)_2$) at high temperature, Fe $(C_5H_5)_2 \rightarrow$ Fe $+H_2 + CH_4 + C_5H_6 + \ldots$ [17]. The reaction product is a closely-packed array of individual multiwalled-carbon-nanotube-encapsulated single-crystal nanowires oriented perpendicular to the substrate. The most commonly observed encapsulated nanowires contain crystallites of α-Fe, γ-Fe, and Fe_3C [11, 12, 15-17]. The presence of γ-Fe is surprising since it is a high temperature phase in the bulk.

*Corresponding author. Email address: m.baxendale@qmul.ac.uk (Mark Baxendale)

In many reports, the nanowires are not continuous but comprise isolated 10s-100s nm length crystallites with a much greater intermediate spacing and the nanotubes have low graphitic quality (as judged by the straightness of the structure.) The growth mechanism is controversial but there is consensus for the general features, usually expressed within a vapour-liquid-solid framework: liquid droplets of elemental Fe accumulate on the substrate, hydrocarbons from the vapour then decompose on its catalytic surface; carbon is absorbed until the solubility limit of carbon in iron is reached; upon saturation, surface carbon is catalytically graphitised by the Fe resulting in multiwalled carbon nanotube growth perpendicular to the substrate. Subsequent growth is driven by supply of iron and carbon species from the vapour either to the base of the structure or to the open tip, or both [17]. The CVD systems employed in the production of these structures generally comprise a horizontal quartz tube inside a two-zone reactor; ferrocene powder is evaporated in the lower-temperature first zone, the vapour is conveyed downstream to the higher-temperature second zone by flowing inert gas (Ar, N_2) where the structures nucleate and grow on the substrates. The temperature of the first zone is selected to favour a controlled evaporation to ensure a regular supply of vapour feedstock to the second zone; that of the second is chosen to thermally decompose the ferrocene, activate the catalytic decomposition of the resultant hydrocarbon species on the surface of substrate-supported Fe droplets, and to promote a high degree of graphitisation in the nanotube walls. The lower temperature limit for the first zone is fixed by the melting point of ferrocene, 175 ^{0}C, that of the second zone is dictated by the temperature range for the decomposition of Fe_3C into α-Fe and graphitic carbon when in contact with a graphitic phase, 600-750 ^{0}C [31]. The fundamentals of this Fe_3C into α-Fe process are unclear but are of great interest in the context of steel corrosion in carbonising gas atmospheres [32]. Direct observation suggests that diffusion of carbon from the nanowire to the nanotube is rate-limited by an intermediate amorphous layer [12].

*Corresponding author. Email address: m.baxendale@qmul.ac.uk (Mark Baxendale)

The presence of Fe_3C in the encapsulated nanowire is, therefore, the result of incomplete diffusion of carbon from within the nanowire to the junction with the nanotube; consequently, quenching of the reaction products has been used to intentionally capture high Fe_3C content [2]. The presence of γ-Fe, which transforms to α-Fe below 912 ^{0}C according to the standard Fe-C phase diagram, usually as a minority component is thought to result from suppression of the γ-α transition, which results in a 9% volume increase, by confinement of the internal nanowire by the high elastic modulus of the carbon nanotube walls (~1 TPa) [12]. Consequently, post-synthesis heat treatment has been the route to both minimising the nanowire carbide content and maximising the γ–Fe content by providing the thermal energy to promote the γ-α transition [33, 34].

A continuous, completely α-Fe nanowire is desirable for some important applications, as is control of both nanowire and nanotube length and diameter. The numerous reports concerning nanowire content control suffer from several major shortcomings: i) the zone-two (synthesis) temperature is expressed as a wide range since the ferrocene vapour is consumed in the sharp temperature gradient at the entrance to the second zone, ii) the post-synthesis cooling rate of the reactor, which could play a critical role in determining the phase content of the nanowire owing to the C-diffusion and γ-α transition arguments expressed above, is seldom quantified or controllable, and iii) little attention is paid to the origin of local diffusion gradients which drive the vapour feedstock to the growth front; often, the tacit assumption is that it is simply concentration driven and occasionally the system-specific, radial temperature gradient between the axis of the vapour-containing tube and substrate is evoked. The temperature-gradient driven model could favour base or tip growth depending on whether the substrate or the vapour is the hotter.

The recent report of a radial Fe-filled carbon nanotube structures departing from a central particle synthesised in fluctuating, flowing vapour produced by the thermal decomposition of

*Corresponding author. Email address: m.baxendale@qmul.ac.uk (Mark Baxendale)

ferrocene points to the temperature gradient produced by hydrocarbon decomposition (exothermic) and graphitic carbon formation (endothermic) at an open tip as that which drives the feedstock to the active growth front when the vapour flow rate is low (~10 sccm) [35]. This conclusion follows from the radial symmetry and analysis of the nanowire composition, full discussion is contained within Ref. 35. Essentially, a low vapour flow-rate facilitates continuous growth by not damping this temperature gradient; thus the balance of growth control is toward the intrinsic features of hydrocarbon decomposition and away from external process parameters. This work is essentially an equivalent study with heterogeneous nucleation (i.e. the nucleating iron particle is formed on a surface) rather than homogeneous nucleation (i.e. nucleating iron particle is formed in the vapour).

Boi *et al* recently concluded that high vapour flow-rate (~100 sccm) promotes high α-Fe content as consequence of driving deposition into a higher temperature region of the reactor to promote C-diffusion and γ-α transitions but at the expense of poor nanowire continuity [36].

With horizontal vapour flow and a perpendicular growth front there will clearly be perturbation of downstream feedstock vapour by upstream structures resulting in degradation of quality. It is known that the nanowire diameter is proportional to that of the nucleating Fe particle and that diffusion of carbon from the nanowire feeds the growth of the nanotube so there is also a scaling of the number of nanotube walls (i.e. nanotube diameter) with encapsulated nanowire diameter [7, 17]. Independent control of these diameters can be achieved either by *ex situ* nanotube filling or introduction of a chlorine-containing precursor and hydrogen [37, 38]. Numerous reports have addressed the question of poor nanowire continuity; Leonhardt *et al.* reported that continuity of is improved by simply increasing the zone-two (synthesis) temperature [7]. Shamsudin *et al*. observed that magnetic properties were highly dependent on changes of synthesis temperature [18]. The diameter of both the

*Corresponding author. Email address: m.baxendale@qmul.ac.uk (Mark Baxendale)

nanowires and nanotubes has been found to scale with the ferrocene evaporation temperature (zone one) close to the melting point temperature, but elevation to ~400 ^{0}C results in vapour-phase nucleation of spherical particles which deposit on the exterior of the nanotube [9,39]. Given the multiple considerations for the selection of the synthesis temperature, the unknown source of to-growth-front diffusion of vapour feedstock, system-specific reporting, and coupled variables, it is not surprising that there is little consensus for universal optimum growth conditions.

We contend that in view of the evidence for the open-tip temperature gradient model at ~10 sccm flow rates, synthesis conditions which favour this condition are desirable since, freed of the necessity to provide a temperature gradient which drives vapour feedstock to the growth front, it facilitates fine-tuning of the synthesis temperature to favour decomposition of Fe_3C into α-Fe and graphitic carbon [35]. Low rates of supply of vapour feedstock also favour low carbide content and the desirable γ–α transition owing to the associated longer residence times (time exposed to elevated temperature). By a similar logic, this regime will guarantee nanowire continuity by providing a local, rather than global, temperature gradient to drive the vapour feedstock to the active growth front. Here, we outline a systematic study of length-diameter, and nanowire content based on ~10 sccm flow rate and a constant close-to-melting-point temperature for the evaporation of ferrocene. The latter consideration is intended to avoid dispersion in the diameter of the nucleating Fe droplet. The synthesis temperature is fixed in narrow range 880 - 950 ^{0}C to encourage C-diffusion but minimise damping of the tip temperature gradient by the natural gradient in the reactor. Under these constrains, the key variable is the mass flow rate of ferrocene vapour into the second zone of the reactor.

Here we report a low vapour flow-rate and constant evaporation temperature method which achieves continuous α-Fe nanowires on the same scale as the nanotube for lengths greater than 10 μm without the necessity of post-synthesis heat-treatment or introduction of other

*Corresponding author. Email address: m.baxendale@qmul.ac.uk (Mark Baxendale)

precursor elements. The magnetic response is comparable to those for structures produced by more complicated syntheses. For initially mixed-phase nanowires of length less than 10 μm, we confirm that continuous α-Fe nanowires can be achieved by post-synthesis heat treatment.

2. Experimental

2.1. Synthesis

The structures were grown on silicon substrates with a thin native oxide layer held within the second zone of a two-zone horizontal CVD reactor. The source vapour was produced by evaporation of ferrocene in the first zone using a coil preheater of low thermal mass to minimise on-off times. The temperature of the preheater was kept constant at 185 ^{0}C by manually adjusting the electrical power delivered to the preheater. The ferrocene vapour was carried from the first to the second zone in an argon flow of 10±2 sccm at atmospheric pressure. The substrates were placed in the second zone in a region in which the lateral temperature gradient was 10 ^{0}C/cm from 880 ^{0}C to 950 ^{0}C. The radial temperature gradient between the axis of the quartz tube and its surface is unknown. The rates of ferrocene vapour mass flow used here (30-50 mg/min.) were calculated by dividing the mass of ferrocene powder loaded into the preheater by the duration time as measured from onset of supply of power to the preheater to the time at which complete evaporation occurred (determined by visual inspection). After the synthesis, the reactor was cooled to room temperature at the natural rate of the furnace (11 hours) and the structures mechanically removed from the substrates.

2.2. Characterization

X-ray diffraction (XRD) analyses were performed using a Siemens D5000 diffractometer and an Xpert-Pro diffractometer (both with Cu Kα source). The Rietveld refinement method,

*Corresponding author. Email address: m.baxendale@qmul.ac.uk (Mark Baxendale)

which applies the least-squares approach to match a theoretical line profile to the diffractogram, was used to identify, and estimate the relative abundances of, the phases contained within the sample from the area enclosed by diffraction peaks. Scanning electron microscopy (SEM) and backscattered electron investigations were performed using an FEI Inspect F system. Transmission electron microscopy (TEM) was performed using a 200 kV Jeol Jem 2010. High resolution transmission electron microscopy (HRTEM) was performed using a 100 kV Nion UltraSTEM 100.The samples for TEM were prepared by dropping small volumes of material dispersed in ethanol onto carbon-coated copper grids followed by drying in ambient conditions. The magnetic measurements were performed at 5 K with a Quantum Design MPMS-7 SQUID magnetometer on the material mechanically removed from the substrates.

3. Results and discussion

Fig. 1 shows typical SEM images of as-grown structures vertically aligned on silicon substrates. Mass flow rates (duration time in brackets) 30 mg/min (1.16 min), 34 mg/min (1.16 min), 39 mg/min (1.5 min), 44 mg/min (1.5 min), and 50 mg/min (1.5 min) has an approximately linear relationship with the nominal length obtained from visual inspection: 3 μm, 5 μm, 10 μm, 15 μm, and 20 μm, respectively.

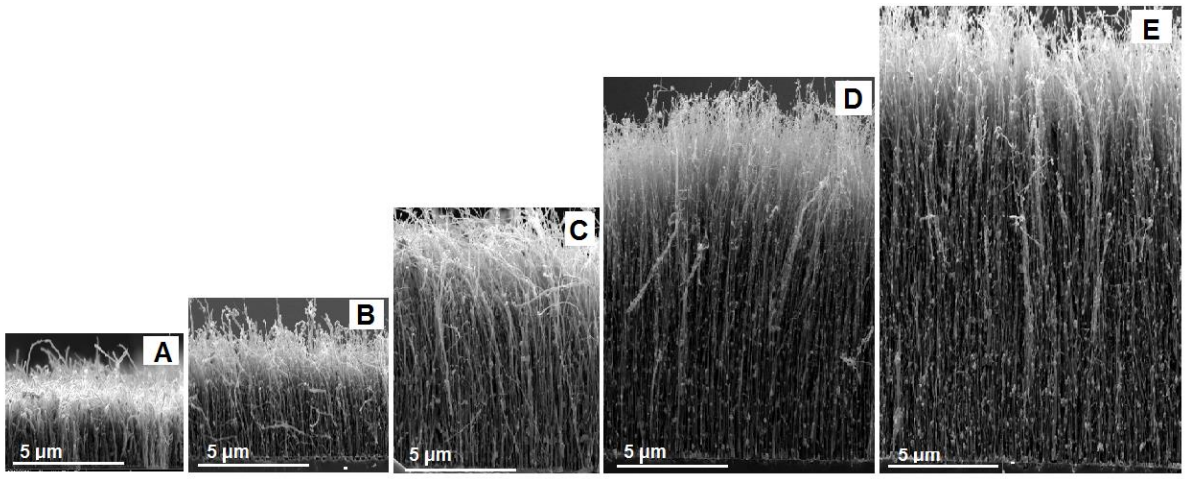

*Corresponding author. Email address: m.baxendale@qmul.ac.uk (Mark Baxendale)

Fig.1. Representative SEM micrographs of structures produced by various rates of ferrocene mass flow: (A) 30 mg/min, (B) 34 mg/min, (C) 39 mg/min, (D) 44 mg/min, and (E) 50 mg/min. The image is of a cross-section through the silicon produced by cleaving through the centre of the substrate.

Compositional analysis of as-grown structures was performed by Rietveld analyses of XRD data, Fig. 2. The common peak at 26.2^0 corresponds to the characteristic 002 reflection of graphitic carbon structure of the multi-walled carbon nanotube, the symmetry and the narrowness of this peak is indicative of the high degree crystallinity. This conclusion is supported by the uniformity and integrity of the nanotube walls directly imaged by HRTEM, Fig. 4 (D, E). The main encapsulated phases were revealed to be those commonly observed, namely α-Fe, γ-Fe and Fe_3C. The presence of the α-Fe in the samples is revealed by observation of the 110 reflection at 44.8^0 while the presence of the γ-Fe is revealed by the 111 and 200 reflections at 43.8^0 and 50.8^0, respectively. Multiple reflections indicative of Fe_3C were observed along with 200, 121 and 211 reflections at 35.3^0, 37.7^0 and 42.9^0, respectively. The dependence of the nanowire composition on length is summarised in Table 1.

*Corresponding author. Email address: m.baxendale@qmul.ac.uk (Mark Baxendale)

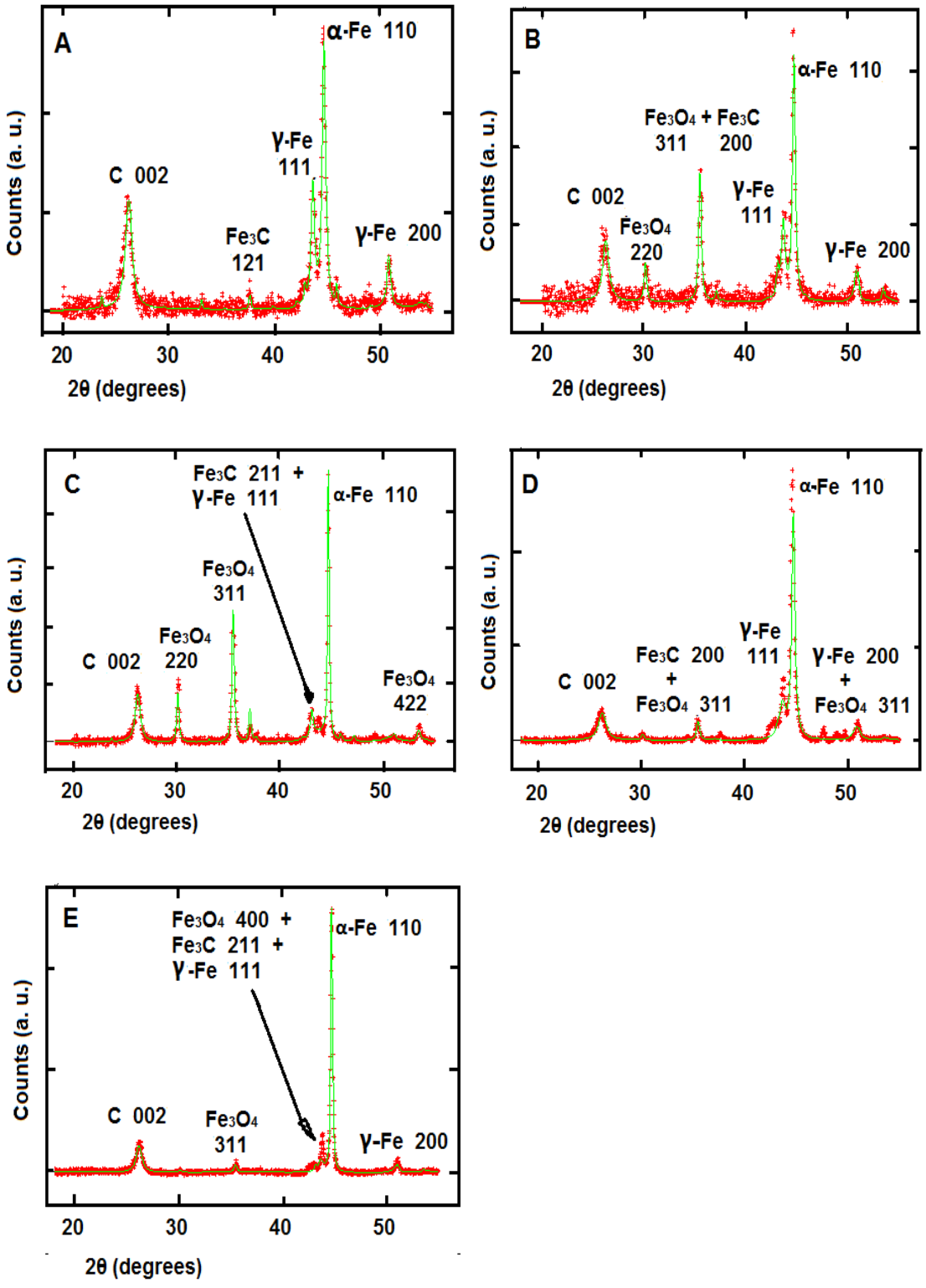

Fig. 2 Typical X-ray diffraction data (red), and Rietveld refinement (green), for lengths 3 µm (A), 5 µm (B), 10 µm (C), 15 µm (D), and 20 µm (E). The refinement was made with the following components α-Fe (Im -3m, Crystal Open Database Ref.64998), γ-Fe (Fm-3m, Crystal Open Database

*Corresponding author. Email address: m.baxendale@qmul.ac.uk (Mark Baxendale)

Ref.9008469), Fe_3C (Pmna, Crystal Open Database Ref.16593), graphitic carbon (P63/mmc, Crystal Open Database Re. 53781), Fe_3O_4 (space group Fd -3m). The origin of oxide components is oxidation of residual elemental iron when the sample is removed from the reactor and handled in air.

Length (μm)	α-Fe (wt.%)	γ-Fe (wt.%)	Fe_3C (wt.%)
3	70	24	6
5	74	22	4
10	94	3	3
15	87	10	3
20	94	5.7	0.3

Table1. Relative abundances of the nanowire phases extracted from the Rietveld refinement of the XRD data in Fig. 2

Clearly there is a step change in α-Fe content, from ~70% to ~90%, as the length increases from 5 μm to 10 μm. The diminution of the γ-Fe and carbide with increasing length is likely to be the consequence of the longer residence time (the length of time at elevated temperature) increasing the probability of γ–α transitions and facilitating carbon diffusion from nanowire to nanotube. An alternative explanation for the diminution of γ-Fe is that these crystallites occur at the ends of the nanowire where confinement effects could be expected to dominate.

The nanowire and nanotube diameter distributions of the 5 μm and 10 μm length were determined from TEM micrographs (examples in Fig.4) of the 5 μm and 10 μm length, Fig.3.

*Corresponding author. Email address: m.baxendale@qmul.ac.uk (Mark Baxendale)

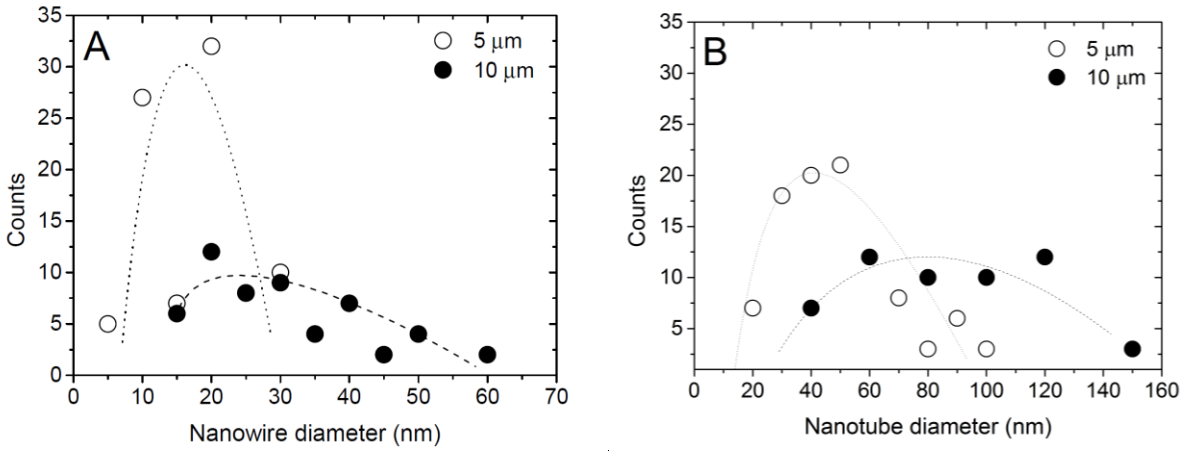

Fig. 3. Diameter distributions for lengths 5μm and 10 μm obtained from direct observation of TEM micrographs: (A) nanowire and (B) nanotube, the dotted lines are guides to the eye. For length 5μm, the average nanowire diameter is 18 nm and that of the nanotube is 48 nm. For the 10 μm structure, the average nanowire diameter is 30 nm and that of the nanotube is 90 nm.

Clearly, there is approximate doubling of both the nanowire and nanotube diameters as the length increases from 5 μm and 10 μm, which is likely to result from the larger nucleating droplet diameter that is the consequence of ferrocene vapour partial pressure as the mass flow rate is increased from 36 mg/min to 44 mg/min. The encapsulating nanowires in the 5 μm and 10 μm length structures are continuous for at least 3 μm and 6 μm, respectively, (Fig. 4 (A-C); the latter value was confirmed by back-scattered electron images of randomly oriented structures, an example is given in Fig. 4(C); the upper encapsulated nanowire (bright region) is continuous for 6 μm. HRTEM images Fig. 4(D, E) show detail of the crystalline structure of the nanowires and nanotube. Note that in contrast to previous reports of intermediate amorphous layers, there is an abrupt interface between the nanowire and nanotube, Fig. 4(E) [12].

*Corresponding author. Email address: m.baxendale@qmul.ac.uk (Mark Baxendale)

The principle of carbide and γ-Fe reduction through post-synthesis heat-treatment mixed-phase nanowires was demonstrated by annealing a powder of 10 µm-long structures at 500 ^{0}C and for 12 hours. The post-heat-treatment XRD and Rietveld analyses revealed a slight increase of α-Fe content from 94% to 98.4% after but reduction of the other phases to negligible amounts, γ-Fe (0.65%) and Fe_3C (0.95%).

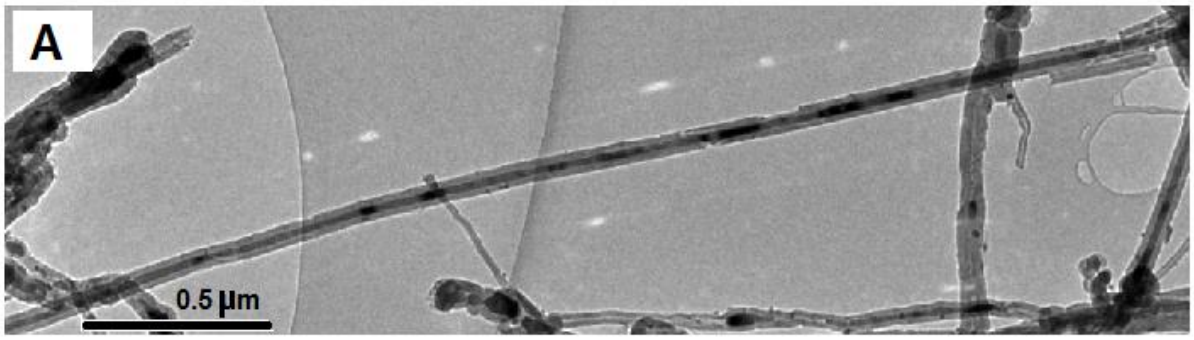

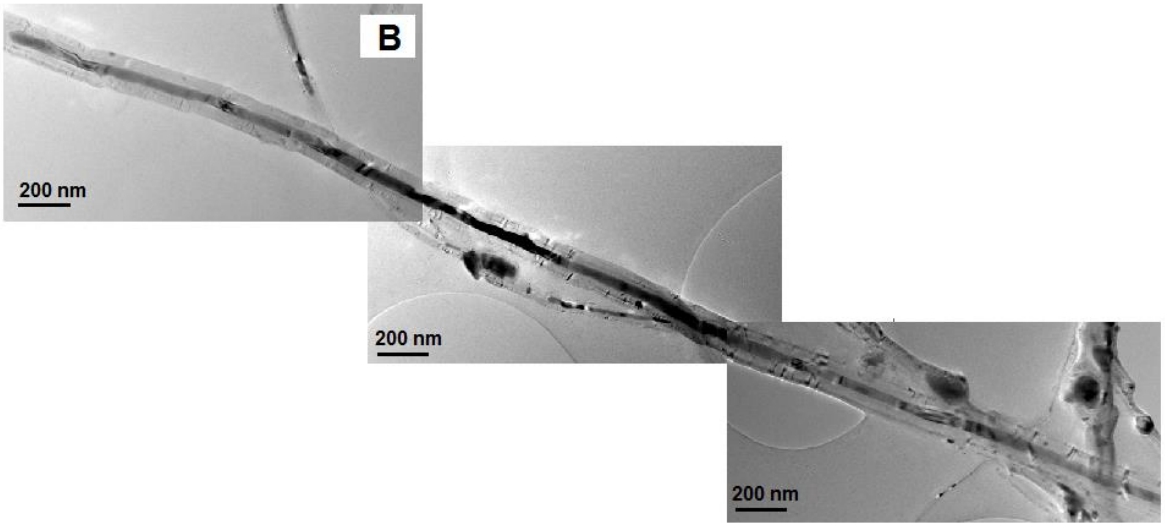

*Corresponding author. Email address: m.baxendale@qmul.ac.uk (Mark Baxendale)

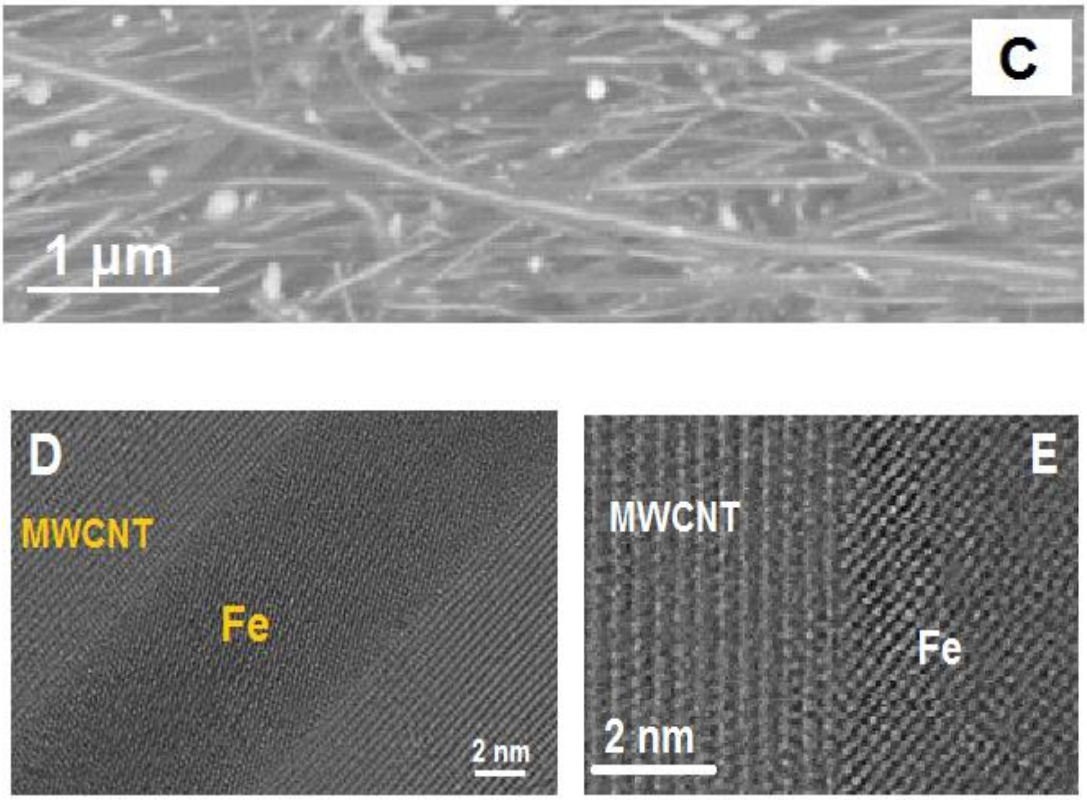

Fig. 4 TEM images 5 µm long structures showing the continuity on the nanowire (A). (B) A sequence of transmission electron micrographs following an individual filled multi-walled carbon nanotube (MWCNT); the filling is continuous for ~ 5 µm. (C) Back-scattered electron image of randomly oriented 10 µm long structures showing the encapsulated nanowire (bright regions), and (D,E) Typical HRTEM images of the 5 µm and 10 µm long samples, respectively; the inter-planar distances of in the nanowire and nanotube, 2 Å and 3.4 Å, correspond to the (110) planes of α-Fe and (002) planes of graphitic carbon, respectively.

The magnetic field dependence of the magnetization of as-grown material in randomly oriented powder form exhibited ferromagnetic hysteresis at 5 K, Fig.5. The saturation magnetization, M_s and coersivity H_c show length dependence. We observed a slight increase of the saturation magnetization with increasing length and a slight decrease of the coercivity, M_s (5µm) = 42 emu/g and M_s (10 µm) = 51.5 emu/g, H_c (5 µm) = 910 Oe and H_c (10 µm) = 846 Oe. Using the same Rietvelt refinement method outlined in Fig.2, the relative

*Corresponding author. Email address: m.baxendale@qmul.ac.uk (Mark Baxendale)

abundances of the components found in the powder comprising 5 μm long structures expressed as wt.% are 65% carbon nanotube, 24% α-Fe, 0.4% γ-Fe, 0.6% Fe_3C, and 10% Fe_3O_4, whereas for 10 μm long structures, 53% carbon nanotube, 32% α-Fe, 0.39% γ-Fe, 0.49% Fe_3C, and 14% Fe_3O_4. Note that the oxide components are a consequence of the oxidation of residual external elemental iron when the sample is removed from the reactor and handled in air; this conclusion follows from direct observation of unencapsulated, approximately spherical, external Fe_3O_4 crystallites by TEM. Based on these result we can say that the increase of the saturation magnetization with increasing the length may be attributed to the greater abundance of ferromagnetic phases (α-Fe, Fe_3C, and Fe_3O_4) in the 10 μm structures compared to that of the 5μm length sample. The coercivity difference can be explained with the increase of the nanowire diameter since the external oxide particles are approximately spherical. A coercivity increase with reduced the diameter has been previously reported [40, 41]. The observed coercivities of 846 Oe and 910 Oe are much higher than that for the bulk polycrystalline Fe (~1 Oe) and nanocrystalline Fe (~23 Oe). The large shape anisotropies of the nanowires can account for the large coercivity. As can the well-known dependence on crystallite dimension (d); for d>30 nm, coercivity is proportional to 1/d and for d<30 nm, coercivity varies as d^{-6} [42, 43].

*Corresponding author. Email address: m.baxendale@qmul.ac.uk (Mark Baxendale)

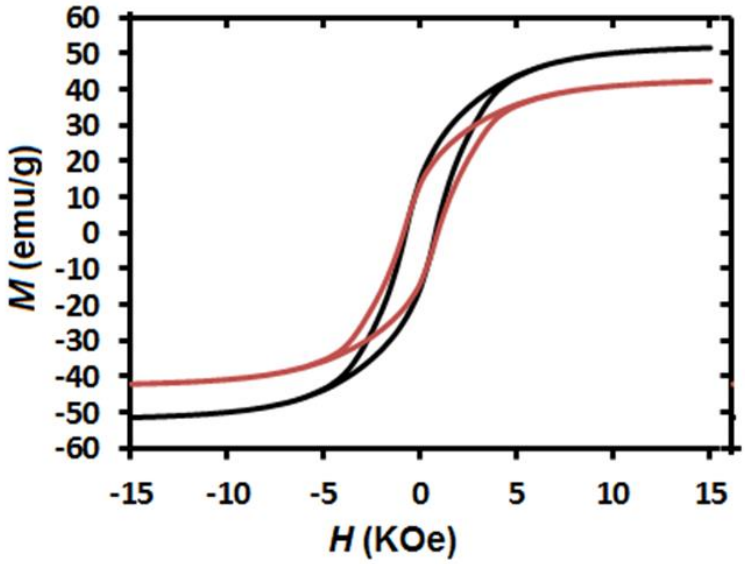

Fig. 5 The magnetic field dependence of dc magnetization at *T* = 5 K for powder comprising 5 µm long structures (red line) and 10 µm long structures (black line).

The saturation magnetisation (M_s = 51.5 emu/g) is the 10 µm length sample at an applied field of 15 kOe. Subtracting the weighted diamagnetic contribution of the carbon nanotube walls, (M_s = -0.7 emu/g) we calculate the combined saturation magnetization of the ferromagnetic material present in our sample (α-Fe, Fe_3C and Fe_3O_4) to be M_s ~ 112 emu/g at 5 K. This value is lower than the estimated saturation magnetization M_s ~181 emu/g at 5 K for a bulk sample corresponding to the same fraction of ferromagnetic components calculated by taking the weighted sum of the saturation magnetization of bulk α-Fe (M_s ~220 emu/g; T_c = 1043 K), Fe_3C (M_s ~169.3 emu/g; T_c = 483 K), and Fe_3O_4 (M_s = 92-100 emu/g; T_c = 850 K) [44, 45, 46]. The lower than expected value of the saturation magnetization has been attributed to the presence of the γ-Fe, which is reported to be antiferromagnetic below 150 K [47]. Since we observe quite low relative abundances of γ-Fe we suggest that geometric factors (grain size, shape, high surface/volume ratio), structural disorder, and surface effects, could contribute to the lowering of M_s below the expected value [48]. Furthermore, superparamagnetism in α–Fe crystallites below the critical dimension would tend to decrease

*Corresponding author. Email address: m.baxendale@qmul.ac.uk (Mark Baxendale)

the measured M_s. Nevertheless the measured M_s values are comparable to those reported in literature by Karmakar *et al*., Dillon *et al*., and Leonhardt *et al*. [47, 49, 50].

4. Conclusion

We conclude that this simple approach to production of continuous α-Fe nanowires encapsulated by multiwalled carbon nanotubes of length greater than 10 μm through thermal decomposition of ferrocene without the necessity of post-synthesis heat treatment or the introduction of other precursor elements yields magnetic responses comparable to those of structures produced by the more complicated synthetic methods. In agreement with previous reports, we confirm that the structures with length less than 10 μm which contain mixed-phase nanowires can be converted to high α-Fe content through post-synthesis heat-treatment.

Acknowledgments

The authors are grateful for the financial support from the Engineering and Physical Science Research Council,UK, and to Rory Wilson, Nadja Tarakina and Richard Thorogate for the help in XRD, TEM and magnetic measurements respectively.

*Corresponding author. Email address: m.baxendale@qmul.ac.uk (Mark Baxendale)

References

[1] Sen R, Govindaraj A, Rao CNR. Carbon nanotubes by the metallocene route. Chem Phys Lett 1997; 267, 276-80.

[2] Setlur AA, Dai JY, Lauerhaas JM, Washington PL, Chang RPH. Formation of graphite encapsulated ferromagnetic particles and a mechanism for their growth. J Mater Res 1998; 13(8): 2139-43.

[3] Rao CNR, Sen R, Satishkumar BC, Govindaraj A. Large aligned-nanotube bundles from ferrocene pyrolysis. Chem Commun 1998; 15:1525-6.

[4] Li DC, Dai L, Huang S, Mau AWH, Wang ZL. Structure and growth of aligned carbon nanotube films by pyrolysis. Chem Phys Lett 2000; 316 (5-6): 349-55.

[5] Marco, JF, Gancedo, JR, Hernando A, Crespo P, Prados C, González, JM, Grobert N, Terrones M, Walton, DRM, Kroto, HW. Mössbauer study of iron-containing carbon nanotubes. 2002; 139-140, 535-42.

[6] Prados C, Crespo P, González JM, Hernando A, Marco JF, Gancedo et al. Hysteresis shift in Fe-filled carbon nanotubes due to γ-Fe. Phys Rev B 2002; 65, 113405-09.

[7] Leonhardt A, Ritchel M, Kozhuharova R, Graff A, Muhl T, Huhle R, et al. Synthesis and properties of filled carbon nanotubes. Diamond Relat Mater 2003; 12(3-7):790-3.

[8] Kuwana K, Saito K. Modelling CVD synthesis of carbon nanotubes: nanoparticle formation from ferrocene. Carbon 2005; 43(10):2088-95.

[9] Leonhardt A, Hampel S, Muller Ch, Monch I, Koseva R, Ritschel M, et al. Synthesis, properties and application of ferromagnetic-filled carbon nanotubes. Chem Vap Deposition 2006; 12: 380-7.

*Corresponding author. Email address: m.baxendale@qmul.ac.uk (Mark Baxendale)

[10] Hampel S, Leonhardt A, Selbmann D, Biedermann K, Elefant D, Muller Ch, et al. Growth and characterization of filled carbon nanotubes with ferromagnetic properties. Carbon 2006; 44: 2316-22.

[11] Muller C, Golberg D, Leonhardt A, Hampel S, Buchner B. Growth studies, TEM and XRD investigations of iron-filled carbon nanotubes. Phys Status Solidi (A) 2006; 203: 1064-8.

[12] Goldberg D, Mitome M, Muller Ch, Tang C, Leonhardt A, Bando Y. Atomic structures of iron-based single-crystalline nanowires crystallized inside multi-walled carbon nanotubes as revealed by analytical electron microscopy. Acta Mater 2006; 54: 2567-76.

[13] Ruskov T, Spirov I, Ritschel M, Muller C, Leonhardt A, Ruskov R. Mossbauer morphological analysis of Fe-filled multiwalled carbon nanotubes samples. J Appl Phys 2006; 100: 084326.

[14] Gui X, Wei J, Wang K, Wang W, Lv R, Chang J, et al. Improved filling rate and enhanced magnetic properties of Fe-filled carbon nanotubes by annealing and magnetic separation. Mater Res Bull 2008; 43: 3441-6.

[15] Weissker U, Loffler M, Wolny F, Lutz MU, Scheerbaum N, Klingeler R, et al. Perpendicular magnetization of long iron carbide nanowires inside carbon nanotubes due to magnetocrystalline anisotropy. J Appl Phys 2009;106:054909.

[16] Lutz MU, Weissker U, Wolny F, Muller C, Loffer M, Muhl T, et al. Magnetic properties of α-Fe and Fe_3C nanowires. J Phys Conf Ser 2010; 200: 072062.

[17] Weissker U, Hampel S, Leonhardt A, Buchner B. Carbon nanotubes filled with ferromagnetic materials. Materials 2010; 3: 4387-427.

*Corresponding author. Email address: m.baxendale@qmul.ac.uk (Mark Baxendale)

[18] Shamsudin MS, Asli NA, Abdullah S, Yahya SYS. Effect of synthesis temperature on the growth iron-filled carbon nanotubes as evidenced by structural, micro-raman, and thermogravimetric analyses. Advances in Cond Matt Phys 2012; 420619.

[19] Dillon FC, Bajpai A, Koos A, Downes S, Aslam Z, Grobert N. Tuning the magnetic properties of iron-filled carbon nanotubes. Carbon 2012; 50: 3674–81.

[20] Lin H, Zhu H, Guo H, Yu L. Investigation of the microwave-absorbing properties of Fe-filled carbon nanotubes. Mat Lett 2007; 61, 3547-50

[21] Hudziak S, Darfeuille A, Zhang R, Peijs T, Mountjoy G, Bertoni G, Baxendale M. Magnetoresistive phenomena on Fe-Filled carbon nanotube/elastomer composites. Nanotechnology 2010; 21(12), 125505

[22] Klingeler R and Sim RB (Eds.) Carbon Nanotubes for Biomedical Applications, Springer 2011.

[23] Klingeler R, Hampel S, Büchner B. Carbon nanotube based biomedical agents for heating, temperature sensoring and drug delivery. Int J Hyperthermia, 2008; 24(6), 496-505

[25] Monch I, Leonhardt A, Meye A, Hampel S, Kozhuharova-Kosera R, Elefant D, et al. Synthesis and characterization of Fe-filled multi-walled carbon nanotubes for biomedical application. J Phys: Conf Ser 2007; 61:820-4.

[25] Ferrari M. Cancer nanotechnology: opportunities and challenges. Nat Rev Cancer 2005; 5:161-71.

[26] Monch I, Meye A, Leonhardt A, Kramer K, Kozhuharova R, Gemming T, et al. Ferromagnetic filled carbon nanotubes and nanoparticles: Synthesis and lipid-mediated delivery into human tumour cells. J Magn Magn Mater 2005; 290-291 (1): 276-8.

*Corresponding author. Email address: m.baxendale@qmul.ac.uk (Mark Baxendale)

[27] Peci T, Dennis T J S and Baxendale M. Iron-filled multi-walled carbon nanotubes surface-functionalized with paramagnetic Gd (III): A candidate dual-functioning MRI contrast agent and magnetic hyperthermia structure. Carbon 2015; 87: 226-32.

[28] Watts PCP, Hsu WK, Randall DP, Kotzeva V, Chen GZ. Fe-Filled carbon nanotubes: Nano-electromagnetic inductors. Chem Mater 2002; 14, 4505-8

[29] Wolny F, Mühl T, Weissker U, Lipert K, Schumann J, Leonhardt, Büchne B. Iron filled carbon nanotubes as novel monopole-like sensors for quantitative magnetic force microscopy. Nanotechnology 2010; 21 435501

[30] Lv R , Tsuge S , Guic X , Takaib K , Kanga F, Enoki T, Weic J , Gua J , Wang K, Wuc D, In situ synthesis and magnetic anisotropy of ferromagnetic buckypaper. Carbon 2009; 47, 1141-5

[31] Schneider A. Iron layer formation during cementite decomposition in carburising atmospheres. Corrosion Science 2002; 44, 2353-65

[32] Callister WD. Fundamentals of materials science and engineering. John Wiley and Sons 2007

[33] Leonhardt A, Ritschel M, Elefant D, Mattern N, Biedermann K, Hampel S, et al. Enhanced magnetism in Fe-filled carbon nanotubes produced by pyrolysis of ferrocene. J Appl Phys 2005; 98: 074315

[34] Gui X, Wei J, Wang K, Wang W, Lv R, Chang J, Kang F,Gu J, Wu D, Mater Res Bull, 2008;43, 3441

[35] Boi FS, Mountjoy G, Baxendale M. Boundary layer chemical vapor synthesis of self-organized radial filled-carbon-nanotube structures. Carbon 2013; 64: 516-26.

*Corresponding author. Email address: m.baxendale@qmul.ac.uk (Mark Baxendale)

[36] Boi FS, Maugeri S, Guo J, Lan M, Wang S, Wen J, et al.Controlling the Quantity of α-Fe inside multiwall carbon nanotubes filled with Fe-based crystals: The key role of vapor flow-rate' Appl Phys Lett 2014; 105, 243108

[37] Jorge J, Flahaut E, Gonzalez-Jimenez F, Gonzalez G, Gonzalez J, Belandria E, et al. Preparation and characterization of a-Fe nanowires located inside double wall carbon nanotubes, Chem Phys Lett 2008; 457, 347-51

[38] Guia X, Wanga K, Wanga,W, Wei J, Zhanga,X, Lvc R, et al. The decisive roles of chlorine-contained precursor and hydrogen for the filling Fe nanowires into carbon nanotubes. Mat Chem Phys 2009; 113, 634-7

[39] Liu Q, Chen Z-G, Liu B, Ren W, Li F, Cong H, Cheng H-M. Synthesis of different magnetic carbon nanostructures by the pyrolysis of ferrocene at different sublimation temperatures. Carbon 2008; 46, 1892-1902

[40] Morelos-Gomez A, Lopez-Urias F, Munoz-Sandoval E, Dennis CL, Shull RD, Terrones H, et al. Controlling high coercivities of ferromagnetic nanowires encapsulated in carbon nanotubes. J Mater Chem 2010;20:5906-14.

[41] Gao JH, Sun DL, Zhan QF, He W, Cheng ZH. Magnetization reversal process and magnetic relaxation of self-assembled Fe_3Pt nanowire arrays with different diameters: Experiment and micromagnetic simulations. Phys Rev B 2007; 75: 064421.

[42] Kersten M. Underlying theory of ferromagnetic hysteresis and coercivity. Z. Phys 1943; 44:63.

*Corresponding author. Email address: m.baxendale@qmul.ac.uk (Mark Baxendale)

[43] Herzer G. Nanocrystalline soft magnetic materials. J Magn Magn Mater 1992;112:258-62.

[44] Tebble S, Craik DJ. Magnetic materials. New York: Wiley;1966.

[45] Haglund J, Grimvall G, Jarlborg T. Electronic structure, x-ray photoemission spectra, and transport properties of Fe_3C (cementite). Phys Rev B 1991; 44(7): 2914–9.

[46] Goya GF, Berquo TS, Fonseca FC, Morales MP. Static and dynamic magnetic properties of spherical magnetite nanoparticles. J Appl Phys 2003; 94(5): 3520–8.

[47] Karmakar S, Sharma SM, Mukadam MD, Yusuf SM, Sood AK. Magnetic behaviour of iron-filled multiwalled carbon nanotubes. J Appl Phys 2005; 97: 054306.

[48] Wang ZH, Zhang ZD, Choi CJ, Kim BK. Structure and magnetic properties of Fe(C) and Co(C) nanocapsules prepared by chemical vapor condensation. J Alloys and Com 2003; 361: 289-293.

[49] Leonhardt A, Ritschel M, Elefant D, Mattern N, Biedermann K, Hampel S, et al. Enhanced magnetism in Fe-filled carbon nanotubes produced by pyrolysis of ferrocene. J Appl Phys 2005; 98: 074315.

[50] Dillon FC, Bajpai A, Koos A, Downes S, Aslam Z, Grobert N. Tuning the magnetic properties of iron-filled carbon nanotubes. Carbon 2012; 50: 3674–81.

*Corresponding author. Email address: m.baxendale@qmul.ac.uk (Mark Baxendale)